J Mater Sci (2007) 42:7423–7432
DOI 10.1007/s10853-007-1835-z

Effect of La substitution on structural and electrical properties of $Ba(Fe_{2/3}W_{1/3})O_3$ nanoceramics

R. N. P. Choudhary · Dillip K. Pradhan · C. M. Tirado · G. E. Bonilla · R. S. Katiyar

Received: 13 April 2006 / Accepted: 22 January 2007 / Published online: 7 June 2007

Abstract The nanocrystalline fine powders (~80 nm) of $(Ba_{1-x}La_x)(Fe_{2/3}W_{1/3})_{1-x/4}O_3$, (BLFW) ($x$ = 0.0, 0.05, 0.10 and 0.15) were synthesized with a combined mechanical activation and conventional high-temperature solid-state reaction methods. Preliminary X-ray structural analysis of pellet samples (prepared from fine powders) showed formation of a single-phase tetragonal system. Detailed studies of dielectric properties (ε_r and tan δ) exhibit that these parameters are strongly dependent on frequency, temperature and La composition. The La-substitution increases the dielectric constant and decreases the tan δ up to 10% substitutions of La at the Ba-site, and then reversed the variation, and hence this composition is considered as a critical composition. This observation was found valid for structure, microstructures, dielectric constant, electrical conductivity, *J–E* characteristics and impedance parameters also. Like in other perovskites (PZT, BZT), La substitution plays an important role in tailoring the properties of $Ba(Fe_{2/3}W_{1/3})O_3$ ceramics.

Introduction

The discovery of high dielectric constant, low tangent loss, high spontaneous polarization and multiple structural phase transitions in $BaTiO_3$ [1] generated a great deal of interest to study perovskite compounds of a general formula ABO_3 (A = mono or divalent, B = tri-*hexavalent* ions) for wide ranging applications, such as transducer, detector, memory and display etc. [2]. Later, discovery of glass-like transition or diffuse phase transition (DPT) with a strong frequency–temperature dependent dielectric dispersion and high dielectric constant in some Pb-based complex perovskites, $Pb(B_{1-x}'B_x'')O_3$ (B′=low-valence and B″=high-valence cations) has attracted much attention for extensive studies of the family for formation of *multilayer* capacitor etc. Some Pb-based Fe^{3+} containing compounds such as $Pb(Fe_{1/2}Nb_{1/2})O_3$, $Pb(Fe_{1/2}Ta_{1/2})O_3$ etc. have shown more interesting features (i.e., electric and magnetic ordering simultaneously in distorted structure) useful for multifunctional devices [3, 4]. Unfortunately, high leakage current and loss tangent, structural instability, etc. limit the material to be used for any practical applications [5]. In order to solve these problems, several attempts have been made including suitable substitutions at the A-and/or B-sites and fabrication of composites/solid-solutions [6]. Though substitutional effects of several isovalent and non-isovalent ions (at the A/B sites) on physical properties of ABO_3-type simple/complex oxides have extensively been studied in the past, partially-substituted La (lanthanum up to 10%) at the A-site has significantly improved (a) ferroelectric/magnetic/multiferroics properties, (b) structural stability, (c) microstructures, (d) density, (e) leakage current etc. of Pb/Ba/Bi- based perovskites [7–8]. Nowadays, Pb-free or low Pb-content materials (environmentally more friendly materials of nanoscale particle size) are of current interest, and hence we have worked on alkaline (group-IIA elements) based materials of a general formula $A(Fe_{2/3}W_{1/3})O_3$ (A = Ba, Sr, Ca, Pb). Literature survey on these materials shows that except some work on multiferroic properties of $BaFeO_3$ [9], not much has been reported as

R. N. P. Choudhary · D. K. Pradhan · C. M. Tirado · G. E. Bonilla · R. S. Katiyar (✉)
Department of Physics, University of Puerto Rico, San Juan, PR 00931, USA
e-mail: rkatiyar@uprrp.edu

yet. In this paper, we report structural, dielectric, electrical, and impedance properties of La-modified $Ba(Fe_{2/3}W_{1/3})O_3$.

Experimental

The polycrystalline samples of La-modified $Ba(Fe_{2/3}W_{1/3})O_3$ (BLFW, i.e., $Ba_{1-x}La_x(Fe_{2/3}W_{1/3})_{1-x/4}O_3$, ($x$ = 0.0, 0.05, 0.10, 0.15)) were prepared using high-purity (≥99.9%, M/s Alpha Aesor Johnson Matthey company) ingredients: $BaCO_3$ (barium carbonate), La_2O_3 (lanthanum oxide), Fe_2O_3 (iron oxide) and WO_3 (tungsten oxide) by four-step synthesis method (i.e., (i) mechanically mixing in wet atmosphere (alcohol), (ii) mechanical activation by high-energy ball-milling (500 rpm, 90 h milling with 15 h interval with 15:1 balls/materials ratio), (iii) high-temperature calcination (1350°C, 4 h) and (iv) high-temperature sintering (1,400 °C for 4 h in air)). The formation of the desired compounds was checked using an X-ray diffraction (XRD) technique. For structural analysis, XRD patterns were recorded in a wide range of Bragg angles, 2θ ($20° \le 2\theta \le 80°$) with a wavelength λ = 1.5405 Å using an X-ray powder diffractometer (*Siemens*, model 5000D) at room temperature (293 K). The grain size/distribution, voids etc. of the pellet samples of BLFW were studied using scanning electron microscope (SEM, JOEL 5800) taken at room temperature. For electrical and dielectric characterization both the parallel surfaces of the pellets were coated with platinum electrode using a dc magnetron sputtering system. The series capacitance (C_s), dissipation factor (D), impedance (Z) and phase angle (φ) of BLFW were obtained as a function of frequency (1 kHz–1 MHz) at different temperatures (300–630 K) using an impedance analyzer (HP 4294A). The leakage current (I–V characteristics) of BLFW was measured as a function of voltage (2–100 V, 2 V steps, 10 s delay time) at an interval of 25 K starting from room temperature (300 K) up to 600 K using a programmable electrometer (Keithley, model 6517A). A cryostat/sample holder along with a programmable-temperature controller (M/S MMR Technologies Inc., model K-20) was used for all the electrical measurements.

Results and discussion

X-ray diffraction analysis

Figure 1 compares the room temperature X-ray diffraction (XRD) patterns of La-modified $Ba(Fe_{2/3}W_{1/3})O_3$ (i.e., $Ba_{1-x}La_x((Fe_{2/3}W_{1/3})_{1-x/4}O_3$, x = 0.0, 0.05, 0.10 and 0.15). The change in the XRD patterns (peak position and intensity) of $Ba(Fe_{2/3}W_{1/3})O_3$ (BFW) on increasing La content is clearly seen. Some peaks of BFW were found splitting on increasing La content, and become single for higher x. All peaks of BLFW (x = 0–0.15) were indexed in cubic, tetragonal and orthorhombic crystal systems and different cell configurations using 2θ value of each peak by a computer software ''POWD'' [10]. The best agreement in experimental and calculated value of d (i.e., $\Sigma(d_{exp} - d_{cal}) = \Sigma\Delta d$ = minimum) was found in the tetragonal system. The least-squares refined lattice parameters of BFW and La-modified BFW (i.e., BLFW) are compared in Table 1. Preliminary structural analysis of BLFW shows that perovskite structure of $BaFeO_3$ (cubic at high temperature) has been distorted to tetragonal on the substitution of W^{6+} at the B-site and La^{3+} at the A-sites. The distortion in structure or unit cell of BLFW can also be studied by calculating Goldsmith tolerance factor [11], $t = (r_A + r_o)/\sqrt{2}\,(r_B - r_o)$, where r_A and r_B are the average ionic radius of A, B site atoms respectively and r_o is the ionic radius of oxygen ions. The calculated value of t varies slightly from 0.99 to 0.98 for x = 0 to 0.15 suggesting the

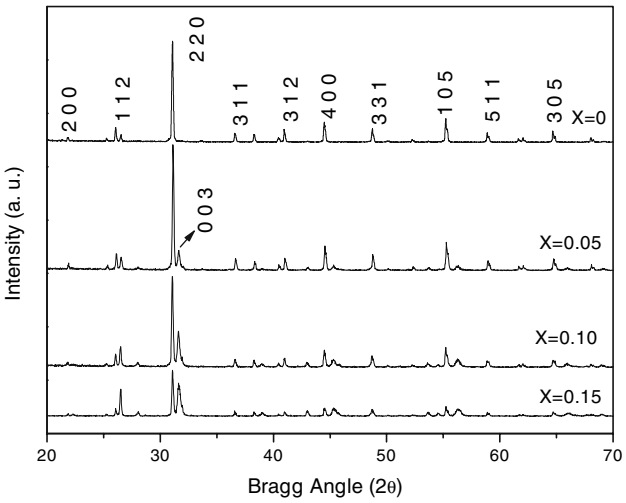

Fig. 1 Room temperature XRD pattern of $(Ba_{1-x}La_x)(Fe_{2/3}W_{1/3})_{1-x/4}O_3$ for different value of x

Table 1 Comparison of lattice parameters (Å), volume (Å^{-3}) and tolerance factor (t) of La-modified $Ba(Fe_{2/3}W_{1/3})O_3$ (i.e., $(Ba_{1-x}La_x)(Fe_{2/3}W_{1/3})_{1-x/4}O_3$)

x	a	c	c/a	V	t
0.00	8.1301 (39)	8.4965 (39)	1.051	561.160	0.99
0.05	8.1026 (36)	8.4815 (36)	1.0468	556.83	0.98
0.10	8.1292 (66)	8.5001 (66)	1.0468	561.72	0.98
0.15	8.1330 (36)	8.4877 (36)	1.0436	561.83	0.97

The estimated standard deviation of the lattice parameters are given parenthesis

stability of the structure. In general, the value of t is ionic-size dependent, and hence creates disordering in the complex system of different sized atoms/ions present at the B-site. The crystallite size of the BLFW samples was calculated using broadening ($\beta_{1/2}$) of a few (peak) reflections of Bragg angle (θ) using Scherrer's equation $P = K\lambda/\beta_{1/2}\cos\theta$ ($K = 0.89$, $\lambda = 1.5405$ Å) [12]. The calculated value of P (ignoring the strain, instrumental and other effect of broadening) for BLFW was found to be approximately ~80 nm.

SEM microstrucutral studies

Figure 2 shows the SEM micrographs of BLFW for different content of La ($x = 0$–0.15). It is observed that the grains are uniformly distributed on the sample surface, and also in the bulk. The average grain size of BFW increases on increasing La content x (up to $x = 0.10$) in BLFW and then decreases. All microstructures show some voids, which confirm the formation of low-density sample (90% of the theoretical density). However, it is clearly seen that La has densified the BFW samples. Cross-sectional micrographs (not shown here) of all the samples were found similar to those of plane surface. This confirms the uniform distribution of grains throughout the bulk samples of PBFW. The microstructures of BLFW with $x = 0.10$ are quite different with large grain size distributed nonuniformly. The grain size and their distribution in the samples for other compositions (i.e., $x = 0$, 0.05 and 0.15) are almost similar.

Dielectric properties

Figure 3 exhibits the variation of relative dielectric permittivity (ε_r) and tan δ (inset) with frequency at some typical temperatures of BLFW. At lower frequencies ($\leq 10^4$ Hz) and high temperatures (≥500 K) ε_r has very high value for pure BFW ($x = 0$), which decreases drastically on substituting La at the Ba-site of BLFW. Generally, the value of ε_r of BLFW increases with increasing La concentration up to $x = 0.1$, and then it decreases. For all the samples, ε_r value decreases on increasing frequency. This is very much consistent for non-linear dielectrics because at lower frequencies all the polarizations (i.e., interfacial, dipole, ionic, atomic and electronic) are present in the samples. The higher value of ε_r for $x = 0.10$ is very much consistent with observed density and microstructures of the samples. This situation is also observed in 10% La substituted $Pb(ZrTi)O_3$ system. The values of tan δ in low-temperature region (≤ 400 K) are almost frequency independent. Generally, tan δ has very high value at low frequency and high temperatures in the Fe containing compounds, which decreases drastically with rise in frequency. The higher value of tan δ, however, decreases faster on increasing La content in BLFW, and hence there is a strong effect of La on ε_r and tan δ values.

The variation of ε_r and tan δ (inset) of BLFW with temperature at few selected frequencies is shown in Fig. 4. The value of ε_r increases with rise in temperature at all the frequencies for all the samples. This increase of ε_r at high frequencies is smaller compared to that of low frequencies. Again ε_r of BFW first decreases for 5% La substitutions,

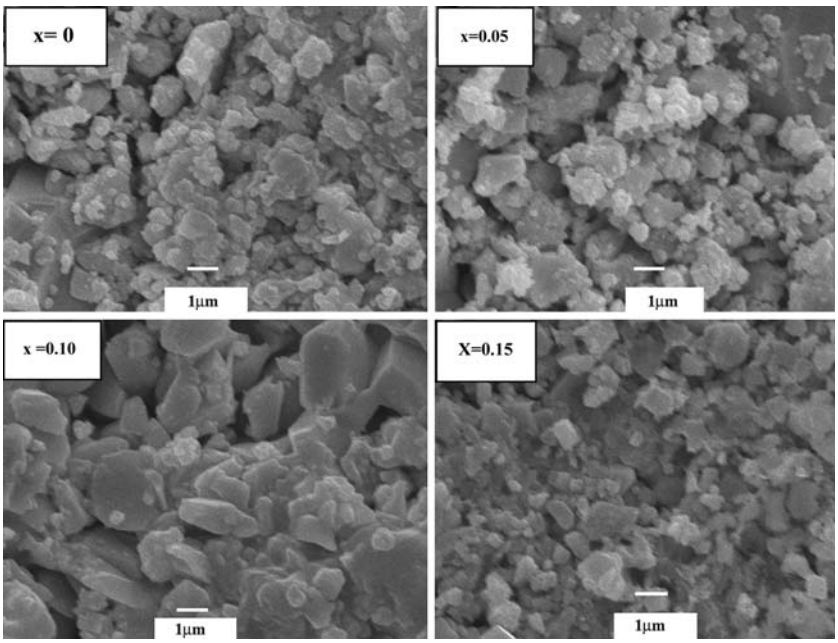

Fig. 2 Room temperature SEM of $(Ba_{1-x}La_x)(Fe_{2/3}W_{1/3})_{1-x/4}O_3$ for different value of $x = 0$, 0.05, 0.10 and 0.15 at magnification (5,000×)

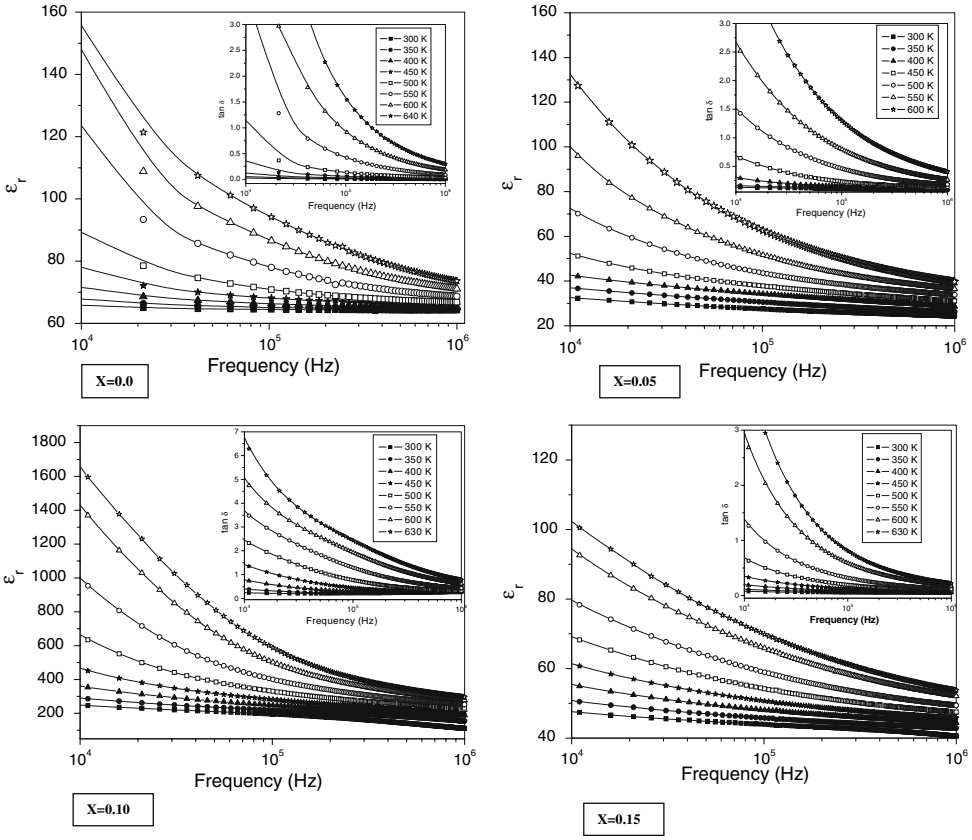

Fig. 3 Variation of relative dielectric permittivity and tan δ (inset) of $(Ba_{1-x}La_x)(Fe_{2/3}W_{1/3})_{1-x/4}O_3$ with frequency at different temperatures for different value of x

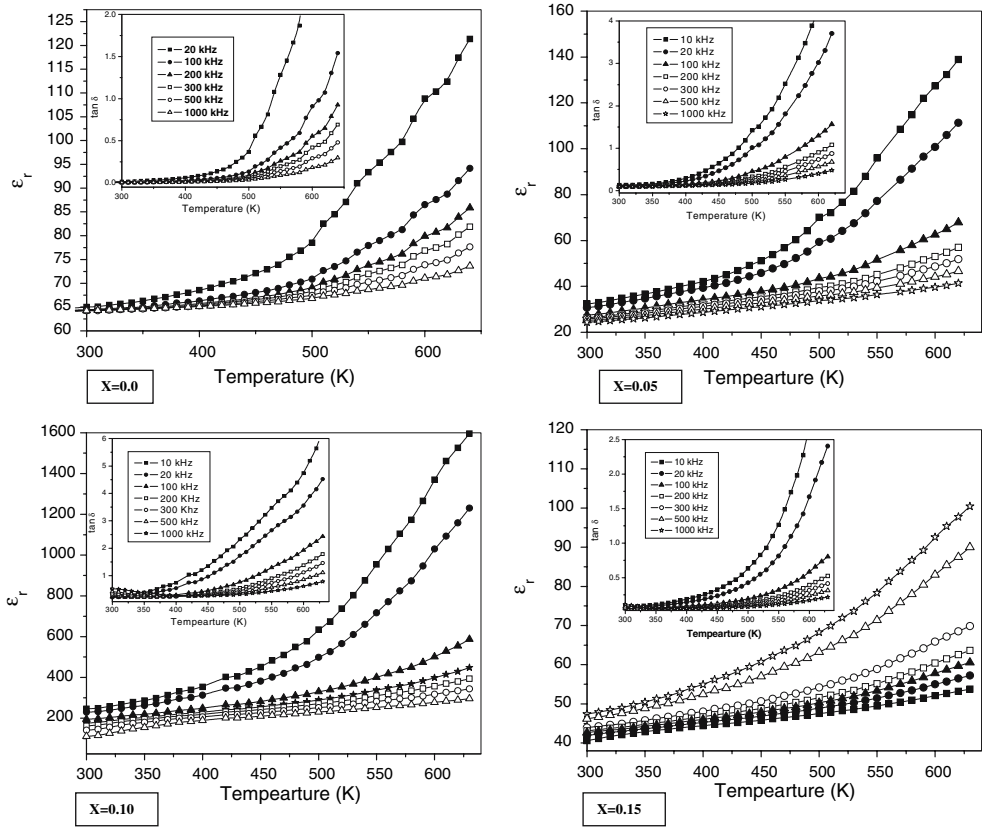

Fig. 4 Comparison of temperature–frequency dependence of relative dielectric permittivity and tan δ (inset) of $(Ba_{1-x}La_x)(Fe_{2/3}W_{1/3})_{1-x/4}O_3$ for x = 0.0, 0.05, 0.10 and 0.15

then drastically increases for $x = 0.10$, and finally decreases sharply for $x = 0.15$. This result suggests that La-substitutions and microstructures have a significant effect on dielectric properties of BLFW with a critical composition of La (i.e., 10%) with higher ε_r value. The value of tan δ below 400 K, is small ($x \leq 0.10$) and almost invariant for BFW. On increasing temperature, tan δ increases very fast particularly at lower frequencies for BLFW. The nature of variation of tan δ with temperature is same as that of ε_r. The values, nature of variation and invariant-temperature region of tan δ are very much compositional (La) dependent. The value of tan δ is also microstructural dependent. For example, for $x = 0.10$, the value of tan δ is higher compared to that of other compositions.

Ac conductivity studies

Figure 5 exhibits the variation of σ_{ac} with frequency at different temperatures (300–640 K). The ac conductivity (σ_{ac}) of BLFW was calculated (from experimental dielectric data) using an empirical relation $\sigma_{ac} = \omega\varepsilon_r\varepsilon_0 \tan\delta$ ($\omega = 2\pi f$ = angular frequency, ε_0 = vacuum permittivity). It has been observed that at low temperatures the conductivity pattern exhibits both low- and high-frequency dispersion, which becomes prominent with increase in La-content (i.e., for BFW the frequency dispersion is almost constant through out the temperature range of investigation). With rise in temperature, high-frequency dispersion of conductivity feature is still retained whereas low-frequency conductivity dispersion showing a plateau like trend. The ac conductivity behavior obeys the Jonscher's power law governed by the relation [13, 14]: $\sigma(\omega) = \sigma_{dc} + A\omega^n$, $0 < n < 1$, where σ_{dc} is the frequency-independent conductivity, A is the temperature-dependent pre-exponential factor and n is the frequency exponent. With gradual rise in temperature the high-frequency conductivity dispersion appears to decrease assuming a plateau like shape preceded by a change in slope in the domain of high frequency. At higher temperatures, the low-frequency plateau corresponds to the dc conductivity of the material, and high-frequency dispersion corresponds to the ac conductivity. For all the La-concentration, dc conductivity increases with increase in temperature. It has been observed that high-frequency dispersion obeying the feature of power law ($\sigma_{ac} \propto \omega^n$) and change in its slope is governed by n. Again σ_{ac} is very much related to the microstructure.

Figure 6 shows the variation of σ_{ac} with temperature at different frequency. The value of σ_{ac} interestingly decreases on decreasing temperature, but increases on increasing La concentration. The activation energy E_a (which is dependent on a thermal activated process) can be calculated using an empirical relation $\sigma_{ac} = \sigma_0 \exp(-E_a/kT)$

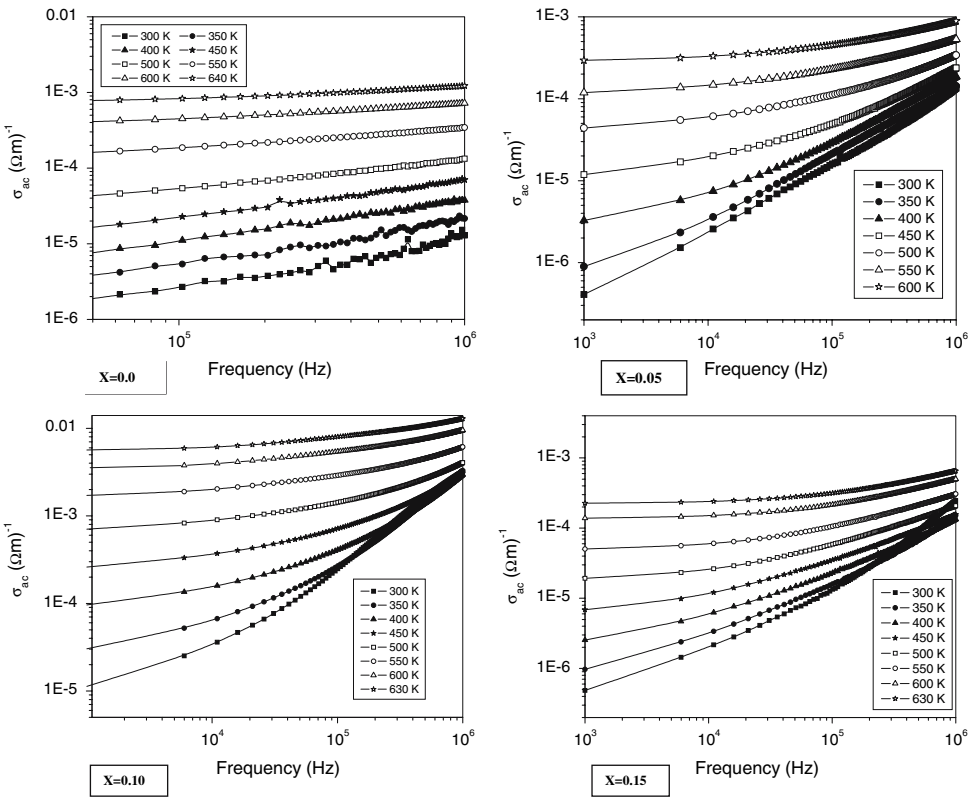

Fig. 5 Frequency dependent of ac electrical conductivity (σ_{ac}) at different temperatures for $(Ba_{1-x}La_x)(Fe_{2/3}W_{1/3})_{1-x/4}O_3$ ceramics for $0 \leq x \leq 0.15$

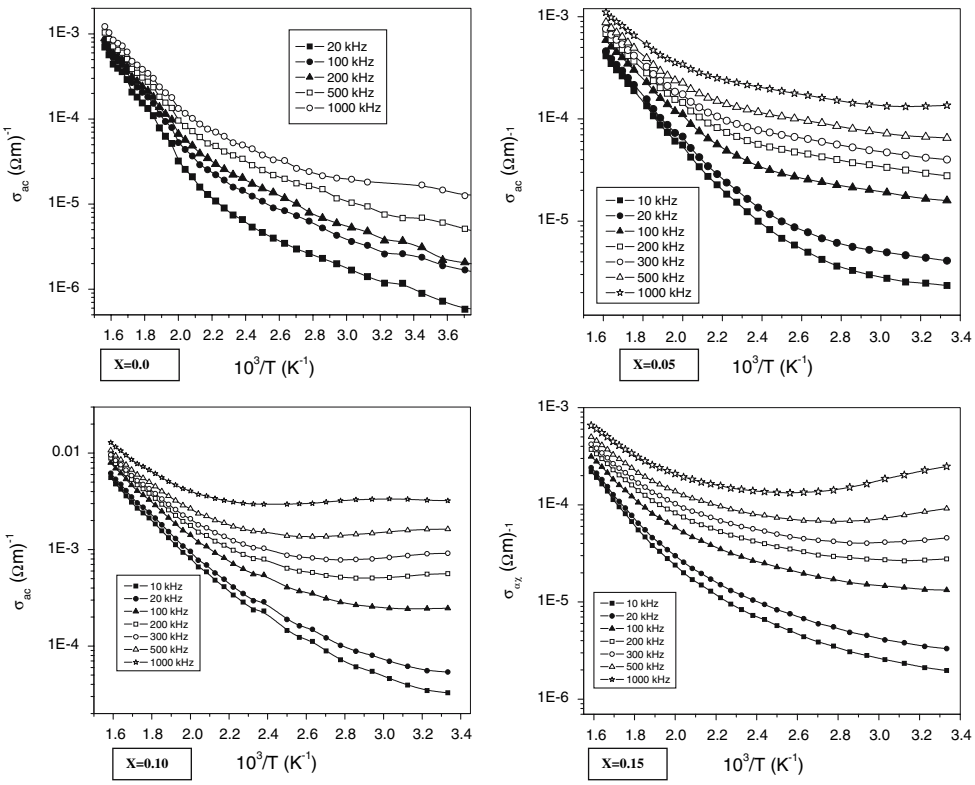

Fig. 6 Temperature dependence of ac electrical conductivity at different frequencies of $(Ba_{1-x}La_x)(Fe_{2/3}W_{1/3})_{1-x/4}O_3$ (x = 0, 0.05, 0.10, 0.15) ceramics

(k = Boltzmann constant, σ_0 = pre-exponential factor). For each frequency in the plot, occurrence of different slopes in the different temperature regions suggests the presence of multiple conduction processes in the samples with different activation energy. At low temperatures and high frequency, ac conductivity is almost independent of temperature, but dependent on frequency. The low activation energy (in low temperature and low frequency) suggests an intrinsic conduction due to the contribution of space charges. The dependence of ac conductivity with frequency is assumed to be due to thermo-ionic electron emission from the trap level of defect center. As we know, space charges are created at the boundary or interface of the samples, and hence polarization fatigue occurs after a few cycle of read/write. From the value of ac conductivity of the samples it is clear that the conduction might be trap-controlled space-charge current conduction.

At high temperature and low frequency, the calculated value of σ_{ac} are very much high compared to that of low temperatures. It is establish that creation of oxygen vacancies gives rise to activation energy of above 1 eV. The higher value of σ_{ac} in higher temperature range shows the predominant role of ionic charge carrier, such as oxygen vacancies (generally created in the ceramics sample during high-temperature sintering). It is found that at high-temperatures σ_{ac} of all the different frequencies merges, and hence it is frequency independent. In the high-temperature and low-frequency regions the value of E_a of BLFW (obtained from the slope of σ_{ac} vs. 1,000/T K^{-1}) was found to be 0.57, 0.45, 0.40 and 0.53 eV for x = 0, 0.05, 0.10 and 0.15 respectively. However, the value of E_a was found to be 0.57, 0.28, 29 and 0.27 eV for the above La compositions of BLFW in the high-temperature high-frequency region. These values also suggest that La has a significant role in conduction process and value of σ_{ac} in BLFW.

Leakage current studies

Figure 7 shows the variation of current density J with electric field E at few selected temperatures. The value of J slowly increases with rise in electric field up to 500 K (for BFW). Above this temperature J has higher value and was not possible to measure up to 800 V/cm. It is found that on increasing La-content in BLFW, leakage current reduces significantly, as observed in BFO ($BiFeO_3$) and other multiferroics. In the low-field region (~100 kV/cm) of J–E characteristic plot, there is a slope of ~1 which indicates that the current conduction is of ohmic-type. In the high-field region, we have a slope greater than one indicating the presence of space-charge limited-current conduction. In the high-electric filed and high-temperature region the conduction process may be considered as a mixture of space charge limited, Schotty and *Frenkel-Poole*. It is clear that vacancies and fatigue play an important role in conduction processes of the system.

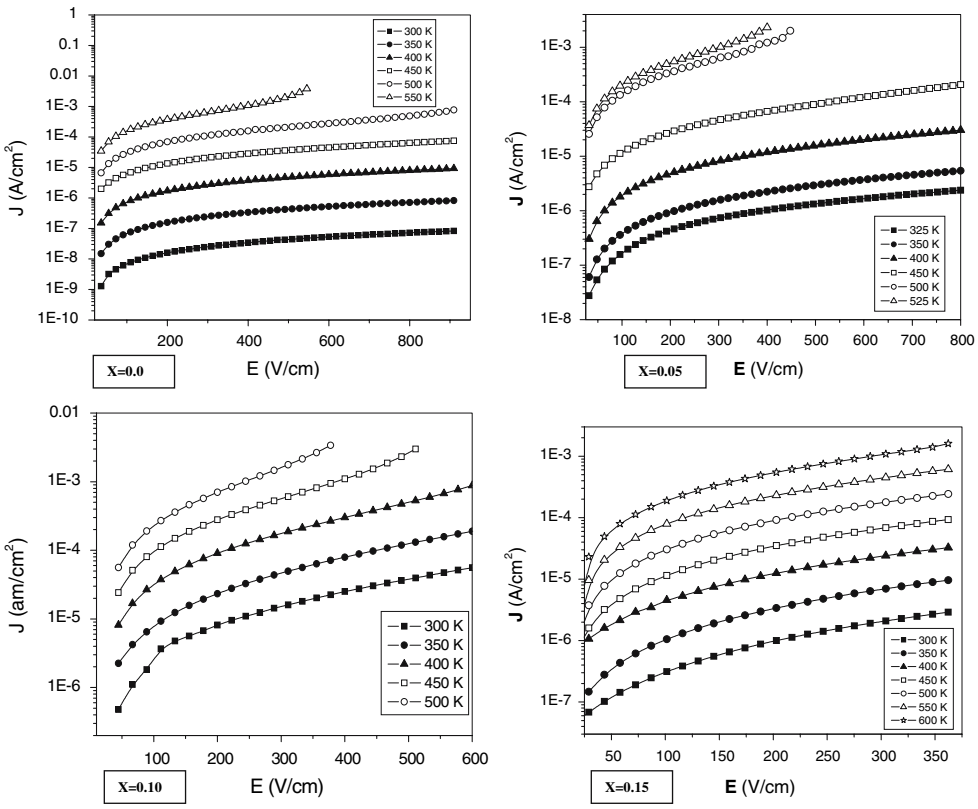

Fig. 7 Variation of current density (J) with electric field (E) at different temperatures of $(Ba_{1-x}La_x)(Fe_{2/3}W_{1/3})_{1-x/4}O_3$ (x = 0, 0.05, 0.10 and 0.15) ceramics

Complex impedance analysis

Complex impedance analysis technique is an important and powerful tool to investigate the electrical properties of materials over a wide range of frequency and temperature. Figure 8 shows the variation of imaginary part of impedance (Z'') with frequency at different temperatures. The Z''-frequency patterns exhibits a few important features such as; (i) a monotonous decrease in Z'' with rise in frequency (without any peak) in the investigated frequency range at low temperatures, (ii) appearance of a peak at a particular frequency (known as relaxation frequency, f_{max}), (iii) decrease in the magnitude of Z'' with a clear shift in the peak frequency towards the higher (frequency) side, and (iv) characteristic peak broadening with rise in temperature. These features may be considered due to occurrence of the temperature-dependent electrical relaxation phenomena in the materials [15]. We also have observed a sudden change in the value of Z'' for x = 0.10, which is consistent with that of microstructure (Fig. 2) and crystal structures (Fig. 1).

The complex impedance spectra (Nyquist-plots) of the BLFW materials obtained at different temperatures are shown in Fig. 9. The complex impedance plot typically comprises of a single semicircular arc, which is gradually resolved with rise in temperature for different amount of La substitutions in BFW. The presence of a single arc in the impedance spectrum (within experimental temperature range) indicates that the electrical process in the BLFW materials arises only due to bulk properties [15]. The bulk resistance (R_b) can be calculated from the intercept of the semicircular axis on the real X-axis. The bulk resistance (dc resistance) of the samples decreases with rise in temperature as indicated by the corresponding reduction in the diameter of the semicircles on increasing temperature. This type of variation in dc resistance with rise in temperature indicates a decrease in the bulk resistivity on rising temperature of the materials, which is an analogous to the negative-temperature coefficient of resistance (NTCR) normally observed in semiconductors.

Figure 10 shows the complex impedance plots, fitted data (by a commercially available software Z Simp Win Version 2) and impedance modulus spectroscopic plots (log Z'', M'' vs log frequency, (inset)) for different La-composition at a particular temperature. The complex impedance plots (Fig. 9) for all compositions comprise of a single semicircular arc with center below the real axis suggesting the departure of process from ideal Debye behavior. This departure is due to the presence of distributed elements in the material electrode system. The angle ($\theta = n(\pi/2)$) by which such a semicircular arc is depressed below the real axis, is related to the width of the relaxation time distribution and other parameters. The

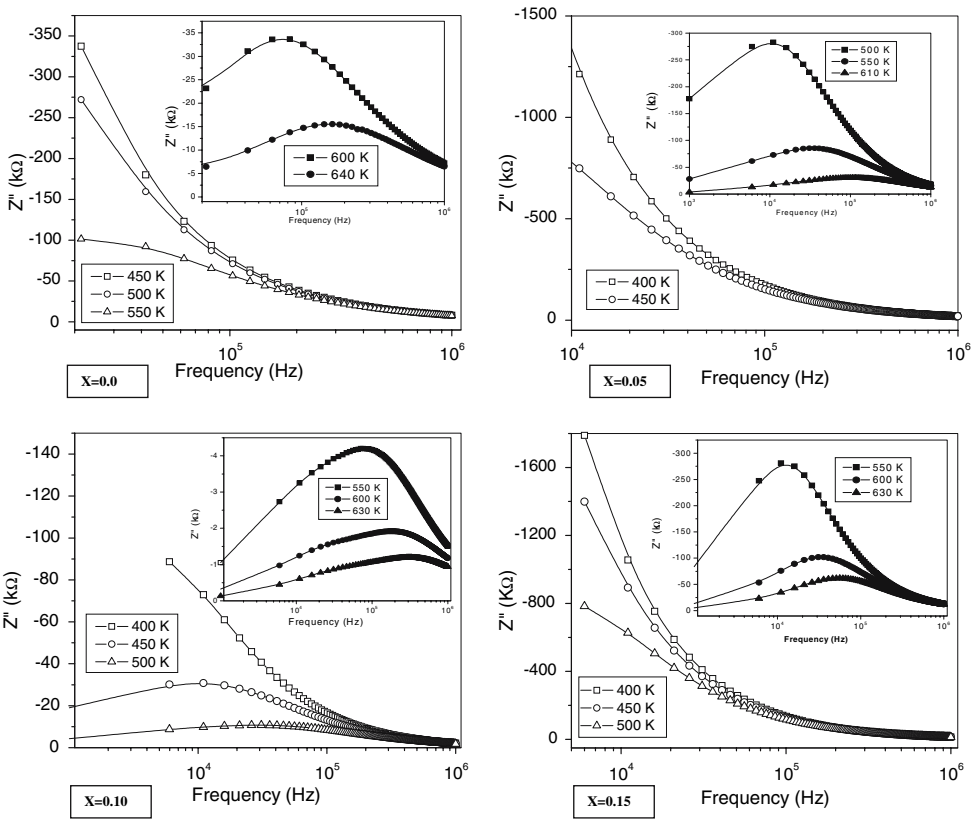

Fig. 8 Variation of imaginary part (Z'') of complex impedance with frequency at different temperatures of $(Ba_{1-x}La_x)(Fe_{2/3}W_{1/3})_{1-x/4}O_3$ ceramics for $x = 0$, 0.05, 0.10 and 0.15

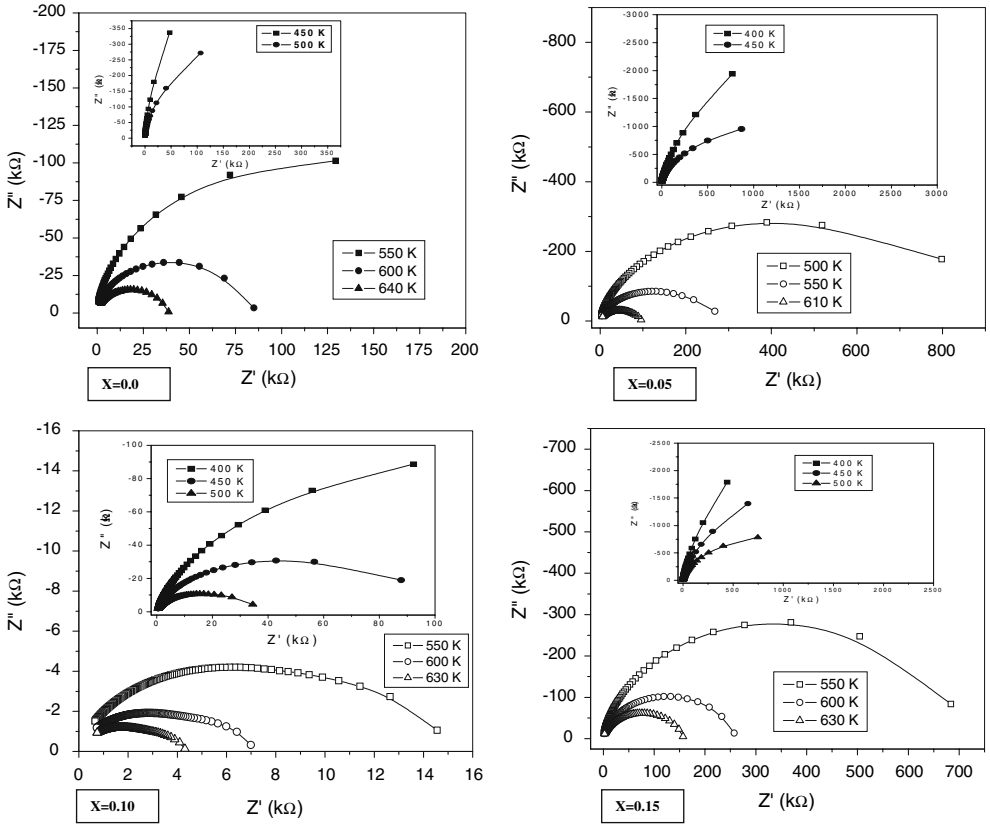

Fig. 9 Effect of La concentration (x) and temperature on impedance spectrum (Nyquist Plot) of La modified $Ba(Fe_{2/3}W_{1/3})_{1-x/4}O_3$

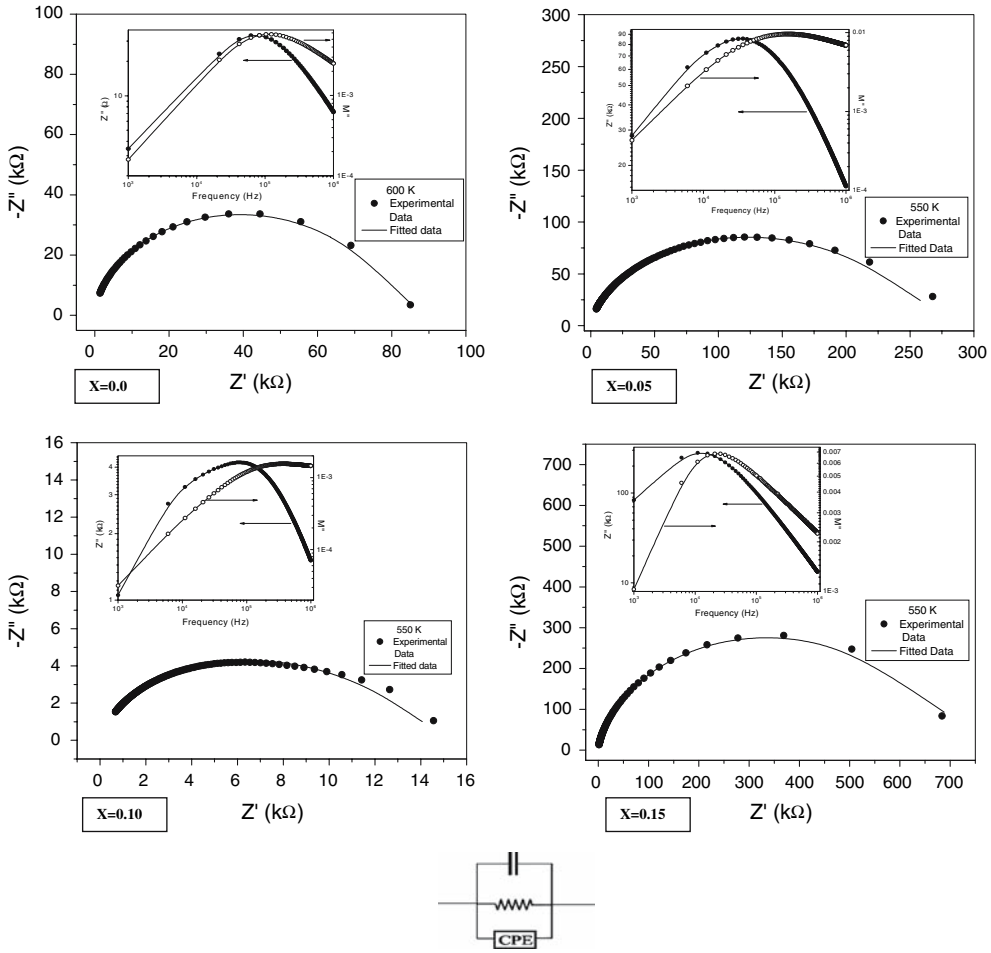

Fig. 10 Comparison of complex impedance plot, fitted data and impedance modulus spectroscopic plot (log Z'', M'' vs log frequency, (inset)) for different La-composition of $(Ba_{1-x}La_x)(Fe_{2/3}W_{1/3})_{1-x/4}O_3$

Table 2 Comparison of temperature dependence of electrical parameters corresponding to the equivalent circuit model by using the fitting processes of the measured data at different temperatures (R_b (Ω), C_b (F), CPE (A_0) and n of $(Ba_{1-x}La_x)(Fe_{2/3}W_{1/3})_{1-x/4}O_3$) ceramics

Composition		Temperature			
		450 K	500 K	550 K	600 K
$x = 0$	R_b	7.14×10^6	1.78×10^6	2.81×10^5	8.91×10^4
	c_b	1.92×10^{-11}	1.94×10^{-11}	1.92×10^{-11}	1.88×10^{-11}
	CPE (A_0)	6.515×10^{-10}	3.67×10^{-9}	5.48×10^{-9}	5.09×10^{-9}
	n	0.65	0.46	0.487	0.52
$x = 0.05$	R_b	2.46×10^6	8.964×10^5	2.798×10^5	1.004×10^5
	c_b	5.51×10^{-12}	6.91×10^{-12}	7.06×10^{-12}	6.76×10^{-12}
	CPE (A_0)	1.176×10^{-10}	1.169×10^{-9}	3.27×10^{-9}	5.136×10^{-9}
	n	0.758	0.597	0.553	0.554
$x = 0.10$	R_b	8.66×10^4	3.27×10^4	1.506×10^4	7.467×10^3
	c_b	3.44×10^{-11}	4.5×10^{-11}	5.91×10^{-11}	6.3×10^{-11}
	CPE (A_0)	2.005×10^{-9}	6.67×10^{-9}	6.383×10^{-8}	2.323×10^{-7}
	n	0.75	0.67	0.527	0.46
$x = 0.15$	R_b	6.014×10^6	1.892×10^6	7.41×10^5	2.712×10^5
	c_b	9.7×10^{-12}	9.6×10^{-12}	9.94×10^{-12}	9.49×10^{-12}
	CPE (A_0)	1.499×10^{-10}	1.729×10^{-10}	4.9×10^{-10}	6.88×10^{-10}
	n	0.70	0.71	0.66	0.67

relaxation time is also not single valued but distributed continuously or discretely around a mean $\tau_m = \omega_m^{-1}$ ($\omega_m = 2\pi f_{max}$). This distribution of relaxation times suggests the presence of constant phase element (CPE) [15]. For ideal Debye-like response, the equivalent circuit comprises of a parallel combination of a resistor and capacitor with single relaxation time. The nature of impedance and modulus spectroscopic plots exhibits the degree of departure from the ideality. It has been found (from the plots) that the Z'' spectra are broadened in the low-frequency side of the peak maxima whereas the M'' spectra broadened in the high-frequency side (i.e., asymmetric peaks). In addition to this, as the maxima of two peaks could not coincide (which are not frequency-coincident), it suggests the departure from the ideal Debye type [16], and hence justify the presence of constant phase element obeying the Jonscher's power law. The CPE admittance is generally represented as: $Y(\mathrm{CPE}) = A_0(j\omega)^n = A\omega^n + jB\omega^n$, [17] where, $A = A_0\cos(n\pi/2)$ and $B = A_0\sin(n\pi/2)$. A_0 and n are frequency independent but temperature-dependent parameters, A_0 determines the magnitude of the dispersion and it varies between zero to one ($0 \leq n \leq 1$). The CPE describes an ideal capacitor for $n = 1$ and an ideal resistor for $n = 0$. In the present study, a single semicircular arc in the impedance spectrum can be modeled to an equivalent circuit of parallel combination of a resistance (bulk resistance), capacitance (bulk capacitance) along with a constant phase element [18]. The values of the temperature-dependent electrical parameters corresponding to the equivalent circuit (shown in Fig. 10) are given in Table 2.

Conclusions

La-substitution, with different composition, plays a significant role in tailoring the structural, dielectric, electrical conductivity, and impedance properties of the $Ba(Fe_{2/3}W_{1/3})O_3$ nanoceramics. La modified BFW has tetragonal (i.e., distorted cubic perovskite) structure. The dielectric parameters (ε_r and $\tan\delta$) are strongly dependent on frequency, temperature and La composition. Complex impedance spectra show the presence of bulk properties for all compositions. Bulk resistance of the La-modified BFW decreases on increasing La concentration. We used an equivalent circuit to explain electrical phenomena occurring inside the materials. The frequency-dependent ac conductivity behavior obeys the Jonscher's power law for all compositions.

Acknowledgement This work was partially supported by the grants no. NASA-NCC3-1034, NSF-0305588 and DoD-W911NF-06-0030. We are thankful to Dr. P. Bhattacharya for some help in experimental works.

References

1. Wul B, Goldman LM (1945) C R Acad Sci URSS 46:139
2. Hill NA, Rabe KM (1999) Phy Rev B 59(13):8759
3. Schmid H (1994) Ferroelectrics 162:317
4. Fiebig M, Lottermoser TH, Frohlich D, Golstev AV, Pisarev RV (2002) Nature (London) 419:818
5. Eorlnskin W, Morrison FD, Dho J, Blamire MG, Scott JF, Mathur D (2005) Science 307:1203a
6. Ryn J, Priya S, Uchino K, Kim HE (2002) J Electroceram 8:107
7. Zhen H, Wang J, Lofland SE, Ma Z, Mohades L et al (2004) Science 303:661
8. Kumar MM, Srinivas A, Suryanarayana SV (2000) J Appl Phys 87:855
9. Matusi T, Taketani E, Fujimura N, Ito T, Morii K (2003) J Appl Phys 93(10):6993
10. ''POWD'' an interactive powder diffraction data interpretation and indexing programme Vs. 2.1, E. WU, School of Physical Sciences, Flinder University of South Australia, Bedford Park, Sau-5402
11. Swartz SL, Shrout TR (1982) Mater Res Bull 17:1245
12. Klung HP, Alexander LB (1974) In: X-ray diffraction procedures. Wiley, New York, p 687
13. Jonscher AK (1977) Nature 267:673
14. Jonscher AK (1983) In: Dielectric relaxation in solids. Chelsea Dielectrics Press, London
15. Macdonald JR (1987) In: Impedance spectroscopy, emphasizing solid materials and systems. Wiley Interscience Publication, New York
16. West AR, Sinclair DC, Hirose N (1997) J Electrocersmics 1:65
17. Macdonald JR (1984) Solid State Ionics 13:147
18. Raymond O, Font R, Suaerz-Almodaver N, Portelles J, Siqueiros JM (2005) J Appl Phys 97:84180